International Journal of Nanomedicine

Dovepress
open access to scientific and medical research

Open Access Full Text Article

ORIGINAL RESEARCH

Intranasal delivery of Huperzine A to the brain using lactoferrin-conjugated N-trimethylated chitosan surface-modified PLGA nanoparticles for treatment of Alzheimer's disease

This article was published in the following Dove Press journal:
International Journal of Nanomedicine

Qingqing Meng,[1,*] Aiping Wang,[1,2,*] Hongchen Hua,[1] Ying Jiang,[1] Yiyun Wang,[1] Hongjie Mu,[1] Zimei Wu,[1] Kaoxiang Sun[1]

[1]School of Pharmacy, Collaborative Innovation Center of Advanced Drug Delivery System and Biotech Drugs in Universities of Shandong, Yantai University, Yantai, People's Republic of China; [2]State Key Laboratory of Long-Acting and Targeting Drug Delivery System, Shandong Luye Pharmaceutical Co., Ltd, Yantai, People's Republic of China

*These authors contributed equally to this work

Correspondence: Kaoxiang Sun
School of Pharmacy, Collaborative Innovation Center of Advanced Drug Delivery System and Biotech Drugs in Universities of Shandong, Yantai University, 30 Qingquan Road, Laishan, Yantai 264005, People's Republic of China
Tel +86 535 394 6400
Email sunkx@ytu.edu.cn

Aiping Wang
School of Pharmacy, Collaborative Innovation Center of Advanced Drug Delivery System and Biotech Drugs in Universities of Shandong, Yantai University, 30 Qingquan Road, Laishan, Yantai 264005, People's Republic of China
Tel +86 535 394 6292
Email wangaiping@luye.com

Background: Safe and effective delivery of therapeutic drugs to the brain is important for successful therapy of Alzheimer's disease (AD).

Purpose: To develop Huperzine A (HupA)-loaded, mucoadhesive and targeted polylactide-co-glycoside (PLGA) nanoparticles (NPs) with surface modification by lactoferrin (Lf)-conjugated N-trimethylated chitosan (TMC) (HupA Lf-TMC NPs) for efficient intranasal delivery of HupA to the brain for AD treatment.

Methods: HupA Lf-TMC NPs were prepared using the emulsion–solvent evaporation method and optimized using the Box–Behnken design. The particle size, zeta potential, drug entrapment efficiency, adhesion and in vitro release behavior were investigated. The cellular uptake was investigated by fluorescence microscopy and flow cytometry. MTT assay was used to evaluate the cytotoxicity of the NPs. In vivo imaging system was used to investigate brain targeting effect of NPs after intranasal administration. The biodistribution of Hup-A NPs after intranasal administration was determined by liquid chromatography–tandem mass spectrometry.

Results: Optimized HupA Lf-TMC NPs had a particle size of 153.2±13.7 nm, polydispersity index of 0.229±0.078, zeta potential of +35.6±5.2 mV, drug entrapment efficiency of 73.8%±5.7%, and sustained release in vitro over a 48 h period. Adsorption of mucin onto Lf-TMC NPs was 86.9%±1.8%, which was significantly higher than that onto PLGA NPs (32.1%±2.5%). HupA Lf-TMC NPs showed lower toxicity in the 16HBE cell line compared with HupA solution. Qualitative and quantitative cellular uptake experiments indicated that accumulation of Lf-TMC NPs was higher than nontargeted analogs in 16HBE and SH-SY5Y cells. In vivo imaging results showed that Lf-TMC NPs exhibited a higher fluorescence intensity in the brain and a longer residence time than nontargeted NPs. After intranasal administration, Lf-TMC NPs facilitated the distribution of HupA in the brain, and the values of the drug targeting index in the mouse olfactory bulb, cerebrum (with hippocampus removal), cerebellum, and hippocampus were about 2.0, 1.6, 1.9, and 1.9, respectively.

Conclusion: Lf-TMC NPs have good sustained-release effect, adhesion and targeting ability, and have a broad application prospect as a nasal drug delivery carrier.

Keywords: Huperzine A, lactoferrin, *N*-trimethyl chitosan, nose-to-brain, nanoparticles, Alzheimer's disease

Introduction

Alzheimer's disease (AD) is the leading cause of age-related dementia, and its prevalence is increasing dramatically because of aging populations worldwide.[1] The direct

and indirect social costs of AD are higher than the expected costs of cancer and cardiovascular disease.[2] AD poses a heavy burden on society and there is an urgent need for effective treatments.[3] Safe and effective delivery of therapeutic drugs to the brain is important for successful AD therapy. However, drug delivery to the brain is challenging because of the presence of the blood–brain barrier (BBB).

As a noninvasive treatment, intranasal administration bypasses the BBB and allows direct access to the brain through olfactory and trigeminal nerve pathways, which has led to its receiving significant attention in recent years.[4,5] It offers advantages such as brain targeting, no gastrointestinal irritation, fast onset of action, avoidance of first pass metabolism, and fewer systemic side effects.[6] However, nasal mucociliary clearance is a significant limiting factor for nasal drug delivery.[7] It severely limits the time available for drug absorption and effectively rules out sustained nasal drug administration.[8]

Mucoadhesive polymers can be used to increase nasal residence time.[8] Chitosan is commonly used as an adhesive for intranasal administration, but it is insoluble and ineffective as a permeation enhancer in a neutral pH environment.[9–11] In contrast, *N*-trimethyl chitosan (TMC) is a quaternized chitosan derivative prepared by reductive methylation, which is positively charged and shows good adhesion and solubility.[12,13] Studies have used these functions to promote mucosal absorption after intranasal administration.[11,14]

Lactoferrin (Lf) has a molecular weight of 80 kDa and is a naturally occurring iron-binding glycoprotein of the transferrin family. Lactoferrin receptor (LfR) is highly expressed on the apical surface of respiratory epithelial cells, as well as in brain endothelial cells and neurons, and particularly overexpressed in capillaries and neurons associated with age-related neurodegenerative diseases, including AD, Parkinson's disease, and amyotrophic lateral sclerosis.[15–17] These findings suggest that Lf is a suitable ligand to mediate enhanced nose-to-brain delivery of formulations after intranasal administration.[18–20]

Huperzine A (HupA) is a reversible inhibitor of acetylcholinesterase (AChE) in a club moss (*Huperzia serrata*), which enhances memory in behavioral animal models.[21–23] Studies have shown that HupA exerts multiple neuroprotective effects in addition to inhibition of AChE.[24–27] HupA has been demonstrated to be clinically useful as a palliative agent for AD in the People's Republic of China and is marketed in the USA as a dietary supplement.[28] However, because of the lack of brain selectivity, commercially available formulations of HupA, such as tablets, capsules, and injections, have serious side effects in gastrointestinal and peripheral cholinergic systems.[29] Therefore, it is highly desirable to use targeted strategies to improve brain-targeted delivery of HupA. In recent years, the utilities of targeted polylactide-co-glycoside (PLGA) nanoparticles (NPs),[30] self-microemulsifying drug delivery systems,[31] nanostructured lipid carriers,[32] and nasal in situ gels[27,33] have been investigated to increase delivery of HupA to the brain. To our knowledge, there are no reports of loading HupA into PLGA NPs for intranasal administration.

Therefore, the objective of this study was to develop HupA-loaded PLGA NPs co-modified with Lf and TMC (Lf-TMC NPs) for efficient intranasal delivery of HupA to the brain for AD treatment. Modification of TMC was expected to increase nasal adhesion and prolong retention time. Conjugation of Lf was expected to facilitate nose-to-brain drug-targeted delivery. The performance of the prepared Lf-TMC NPs was evaluated in vitro by various criteria, ex vivo by cytotoxic properties, and in vivo by imaging the biodistribution in mice.

Methods

Materials and animals

PLGA 5050 2A (lactide/glycolide ratio 50/50; molecular weight 18,000 Da) was purchased from Lakeshore Biomaterials (Birmingham, AL, USA). Chitosan with a degree of deacetylation greater than 90% was obtained from Haidebei Marine Bioengineering (Jinan, People's Republic of China). *N*-Succinimidyl 3-maleimidopropionate (SMP) and coumarin-6 were purchased from Aladdin (Shanghai, People's Republic of China). HupA was supplied by WEPON (Zhejiang, People's Republic of China). Porcine mucin (PM) was purchased from Baoman Bio (Shanghai, People's Republic of China). Lf, 2-iminothiolane (Traut's reagent) and 5,5-dithiobis-(2-nitrobenzoic acid) (Ellman's reagent) were provided by Sigma-Aldrich Co. (St Louis, MO, USA). A bicinchoninic acid (BCA) protein quantitation kit was purchased from Beyotime Biotechnology (Shanghai, People's Republic of China). Nile red, 1,1-dioctadecyl-3,3,3,3-tetramethylindotricarbocyanineiodid (DiR), and 2′-(4-ethoxyphenyl)-5-(4-methyl-1-piperazinyl)-2,5′-bi-1H-benzimidazole trihydrochloride (Hoechst 33342) were purchased from Fanbo Biochemicals Co. (Beijing, People's Republic of China). DMEM and heat-inactivated fetal bovine serum (FBS) were purchased from Thermo Fisher Scientific (Waltham, MA, USA). All other reagents were analytical grade. 16HBE and SH-SY5Y cell lines were provided by

the American Type Culture Collection (ATCC; Beijing Zhongyuan, Beijing People's Republic of China). Kunming (KM) mice (male; age: 4–5 weeks; weight: 20±2 g) were a gift from Luye Pharma Group (Shandong, People's Republic of China).

All animal studies were conducted in accordance with the Laboratory Animal Care and Use Guidelines and approved by the Animal Ethics Committee of Yantai University.

Synthesis and characterization of the conjugated polymers

The synthetic routes to TMC and maleimide–TMC (Mal-TMC) are shown in Figure 1. TMC was synthesized as described previously.[34] In brief, chitosan was mixed with methyl iodide in a basic solution of *N*-methylpyrrolidinone at 60°C for 1 h. The product was precipitated using ethanol and subsequently isolated by centrifugation. The precipitate was collected and dissolved in a 10% (w/v) NaCl solution to replace iodide with chloride. The suspension was dialyzed against deionized water for 3 days to remove inorganic material. Finally, the product was collected by lyophilization (Freeze Dry System; Labconco, Kansas, MO, USA) to generate a TMC powder. Mal-TMC was synthesized via the reaction of TMC and SMP.[35] In brief, TMC was dissolved in 4-(2-hydroxyethyl)-1-piperazineethanesulfonic acid (HEPES) buffer. A solution of SMP in dimethyl sulfoxide (DMSO) was added dropwise to the HEPES solution, and the mixture was stirred at room temperature for 8 h. After dialyzing against deionized water for 24 h, the reaction product (Mal-TMC) was collected by lyophilization.

TMC and Mal-TMC were characterized using a ^{1}H-nuclear magnetic resonance (NMR) spectrum spectrometer (Advance Bruker 400M; Switzerland Bruker Company, Madison, WI, USA). The degrees of quaternization were calculated as follows:

$$DQ(\%) = \left\{ \frac{\int[(CH_3)_3]}{\int(H1)} \times \frac{1}{9} \right\} \times 100 \quad (1)$$

where DQ (%) is the degree of quaternization as a percentage, $\int[(CH_3)_3]$ is the integral of the quaternary amino group peaks, and $\int(H1)$ is the integral of the ^{1}H peaks.

The degree of functionalization of the TMC with maleimide groups was analyzed by high-performance liquid chromatography (HPLC, LC-20A VP System; Shimadzu, Kyoto, Japan) at the end of the reaction. HPLC was performed using an Inertsil ODS-2 C18 column (4.6×250 mm, 5.0 µm). The mobile phase consisted of 16% acetonitrile containing 0.1% trifluoroacetic acid. The flow rate was 1.0 mL/min. Ultraviolet (UV) detection was performed at 220 nm.

Preparation and formula optimization of HupA-loaded NPs

Preparation of NPs

HupA-loaded PLGA NPs (HupA PLGA NPs) were prepared using the emulsion–solvent evaporation method as described previously with slight modification.[12] In detail, 10 mg PLGA and 1 mg HupA were dissolved in 1 mL acetone and dichloromethane (1:4) as the organic phase. The organic phase was then added dropwise to 7.5 mL of 1% polyvinyl alcohol (PVA) in deionized water, followed by ultrasound sonication (200 W) for 100 s in an ice bath and continued stirring for 4 h to evaporate the organic solvent. The NPs were collected by centrifugation and washed with deionized water three times to remove free HupA.

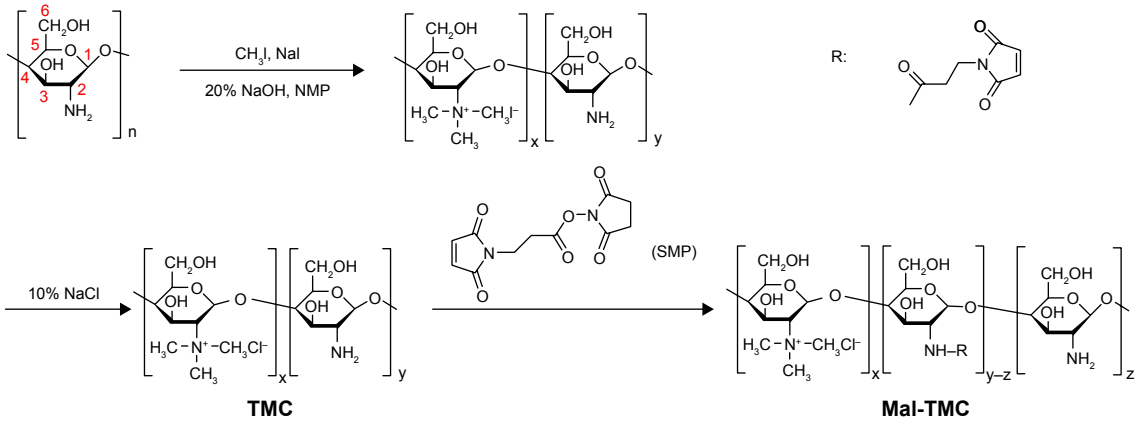

Figure 1 The synthesis routes of TMC and Mal-TMC.
Note: R represents the maleimide group.
Abbreviations: TMC, N-trimethylated chitosan; Mal-TMC, maleimide–TMC; SMP, *N*-Succinimidyl 3-maleimidopropionate.

HupA TMC NPs were prepared by the same method except that Mal-TMC (3 mg) was dissolved in 7.5 mL of a 1% (w/v) PVA solution as the aqueous phase.[12]

Box–Behnken experimental design

To optimize the preparation process and determine the effect of various factors on the encapsulation efficiency and particle size of TMC NPs, a three-factor, two-level Box–Behnken design was used based on preliminary experimental data.[36] A total of 17 confirmatory formulation runs were generated with five center points using Design-Expert® software (version 8.0.0; Stat-Ease, Minneapolis, MN, USA). Table 1 shows the levels of independent and dependent variables. The influence of independent process-dependent variables on the response was assessed using the second order polynomial equation.

Preparation of Lf-TMC NPs

Lf was thiolated by reacting with a 40:1 M excess of Traut's reagent for 60 min, according to Huwyler's method.[37] The products were purified using a Sephadex G25 column. The amount of introduced thiol groups was measured by UV spectrophotometry (X-2; Metash Instruments Co., Shanghai, People's Republic of China) (λ=412 nm) with Ellmann's reagent. The purified thiolated protein was mixed with TMC NPs at a molar ratio of 1:5 (Lf:maleimide). The reaction was allowed to continue for 8 h at room temperature. The incubating medium was HEPES and NaCl solutions (pH 7.0). The products were centrifuged at 12,000 rpm for 30 min to remove unconjugated proteins. The protein conjugation efficiency was assessed using the BCA protein quantitation kit.

Nile red-, coumarin-6-, and DiR-loaded NPs were prepared using the same approach. All NPs were washed three times with ultrapure water and collected by centrifugation.

Characterization of NPs

Particle size, size distribution, and zeta potential

A dynamic light scattering (DLS) particle size analyzer (Deisa TM Nano C; Beckman Coulter, Brea, CA, USA) was used to measure the average diameter, polydispersity index, and zeta potential of the NPs.

Table 1 Different levels of variables in the Box–Behnken design

Variables	Level		
	Low	Medium	High
Independent variables			
A = Polymer concentration (mg/mL)	2.5	6.25	10
B = Theoretical drug loading (%)	5	15	25
C = PVA concentration (mg/100 mL)	0.5	1	1.5
Dependent variables	Desired constraints		
Y_1 = Entrapment efficiency (%)	Maximize		
Y_2 = Diameter of particles (nm)	Minimize		

Abbreviation: PVA, polyvinyl alcohol.

Determination of entrapment efficiency (EE) of NPs

Ultrafiltration was used to determine the EE of NPs. In detail, samples were placed in an ultrafiltration device (100 kDa MWCO; Sartorius, Göttingen, Germany) and centrifuged at 3,600 rpm for 10 min at 4°C to isolate the free drug. The same volume of each sample was then dissolved in methanol to determine the total drug content. The obtained solution was filtered through a 0.45 μm microporous filtering film and then analyzed by HPLC. The mobile phase consisted of methanol and 0.2% H_3PO_4 (25:75, v/v). The flow rate was maintained at 0.8 mL/min and UV detection was performed at 310 nm. The EE of NPs was calculated using the following equation:

$$\text{EE}(\%) = \frac{\text{Total amount of drug} - \text{Amount of free drug}}{\text{Drug dosage}} \times 100 \quad (2)$$

In vitro drug release study

Cellulose membrane dialysis bags were used to investigate the release of HupA from NPs.[30] The in vitro release profiles of HupA-loaded NPs were measured at 37°C in 40 mL of 0.1 M PBS (pH 7.4) for 96 h. The concentration of HupA in the samples was analyzed by HPLC as described.

Adsorption of mucin onto NPs

Adsorption of mucin onto NPs was determined using a previously described method.[11,38] In brief, 5 mL of each PM suspension (0.5 mg/mL PM in PBS, pH 7.4) and NPs (2 mg/mL) were mixed for 1 h at 37°C, followed by centrifugation at 10,000 rpm for 1 h at 4°C. Then, the free PM concentration in the supernatant was determined using a UV spectrometer at a wavelength of 253 nm. The mucin binding efficiency (%) of the NPs was calculated using the formula:

$$\text{Mucin binding efficiency}(\%) = \frac{\text{Total mucin} - \text{Free mucin}}{\text{Total mucin}} \times 100 \quad (3)$$

Cellular studies of NPs

Cytotoxicity of NPs

An MTT assay was used to detect the effect of various NPs on cell proliferation. In brief, 16HBE cells were seeded into a 96-well plate (5×10^3 cells in 200 μL per well) and incubated for 24 h. The cells were exposed to various concentrations of blank or HupA-loaded NPs at 37°C with 5% CO_2 for 24 h.

MTT solution (100 µL) was added to each well, followed by incubation at 37°C for 4 h. The resulting formazan crystals were dissolved in 100 µL DMSO. The absorbance of each well was measured at 570 nm after gentle shaking for 10 min. Cell viability was determined by comparing the absorbance of NP-treated cells with that of control samples.

Cellular uptake of NPs

Qualitative analyses of cellular internalization of Nile red-loaded NPs were carried out by fluorescence microscopy (Eclipse E400; Nikon Corporation, Tokyo, Japan), whereas quantitative analyses of coumarin-6-loaded NPs were carried out by flow cytometry (BD Accuri C6; BD Biosciences, San Jose, CA, USA).

For fluorescence microscopy, 16HBE and SH-SY5Y cells were seeded into 24-well plates (2×10^4 cells in 1 mL medium per well) and incubated at 37°C with 5% CO_2. After cultivation for 24 h, the cells were incubated with Nile red-loaded NPs (1 µg/mL) for various times. Subsequently, the cells were washed three times with cold PBS and fixed with 4% paraformaldehyde for 10 min. To label the cell nucleus as a reference for the intracellular localization of NPs, the cells were further incubated with Hoechst 33342 for 10 min. Finally, the cells were washed three times and visualized by fluorescence microscopy.

For flow cytometry, 16HBE and SH-SY5Y cells were seeded into 6-well plates (8×10^5 cells in 2 mL medium per well) and treated as described above. The culture medium was replaced with 2 mL of medium containing various NPs (coumarin-6 PLGA NPs, coumarin-6 TMC NPs and coumarin-6 Lf-TMC NPs; the coumarin-6 concentration in the NPs was 3 ng/mL). The cells were washed three times with cold PBS after 15, 30, 60, 90, and 120 min of incubation at 37°C. The cells were then trypsinized and centrifuged at 1,500 rpm for 5 min. Finally, the cells were washed three times and analyzed by flow cytometry. The mean cellular uptake-related fluorescence intensity was calculated. Cells to which no NPs were added were used as the control group.

In vivo imaging

KM mice were randomized into three groups and treated intranasally with DiR-loaded PLGA, TMC, or Lf-TMC NPs. Three mice for each formulation per time-point (0.5, 1, 4, and 8 h) were used in the study. For intranasal administration of NPs, a capillary-end gel-loading pipette tip (Corning Inc., Corning, NY, USA) attached to a pipette containing a DiR dose of 0.5 mg/kg was inserted approximately 10 mm into the mouse nasal cavity. The live mice were monitored at various time-points, and images of organs were obtained at the final time-point using the In-Vivo Imaging System FX Pro (Carestream, NY, USA) with an excitation wavelength of 720 nm and emission wavelength of 790 nm. Before administration and imaging, mice were anesthetized by intraperitoneal injection of chloral hydrate. The images were analyzed using Carestream Image Suite Software.

Biodistribution study

KM mice were randomly divided into three groups for intranasal administration of HupA-loaded PLGA, TMC, and Lf-TMC NPs. Three mice were used for each formulation per time-point (0.25, 1, 2, 4, 8, and 12 h). Blood samples were collected at each time-point from the eyes of mice, and the mice were killed for dissection of the olfactory bulb, hippocampus, cerebrum with hippocampus removed, and cerebellum. The blood samples were centrifuged at 1,500 rpm for 10 min to isolate the plasma. Other tissues were homogenized after adding three volumes of saline. To extract the HupA, 1 mL ethyl acetate was added to the alkalized plasma or tissue homogenate. The HupA concentration was measured by liquid chromatography–tandem mass spectrometry (LC-MS/MS) (AB Sciex Triple Quad™ 4500; Sciex, Framingham, MA, USA). The LC-MS/MS conditions were as follows: chromatographic column, Shim-pack XR-ODS III C18; mass spectrometer ion source, electrospray ionization source; HupA ion pair, 234.4/210.1. HupA concentrations were normalized to the dose and plotted as concentration–time curves. WinNonlin software (version 6.4; Certara, Princeton, NJ, USA) was used to calculate the pharmacokinetic parameters. The areas under the curve (AUCs) of HupA in the brain and blood were calculated separately. The drug targeting index (DTI) was calculated to evaluate brain-targeting efficiency. DTI values were calculated as follows:

$$DTI = \frac{(AUC_{brain}/AUC_{plasma})\ NPs}{(AUC_{brain}/AUC_{plasma})\ PLGA\ NPs} \quad (4)$$

Statistical analysis

Data are presented as the mean ± SD. The Student's *t*-test and one-way analysis of variance (ANOVA) were used to determine the significance between two groups and among more than two groups, respectively.

Results and discussion

Characterization of TMC and Mal-TMC

^{1}H-NMR spectrum

TMC and Mal-TMC syntheses were confirmed by ^{1}H-NMR (Figure 2). As shown in Figure 2A, the chemical shifts of

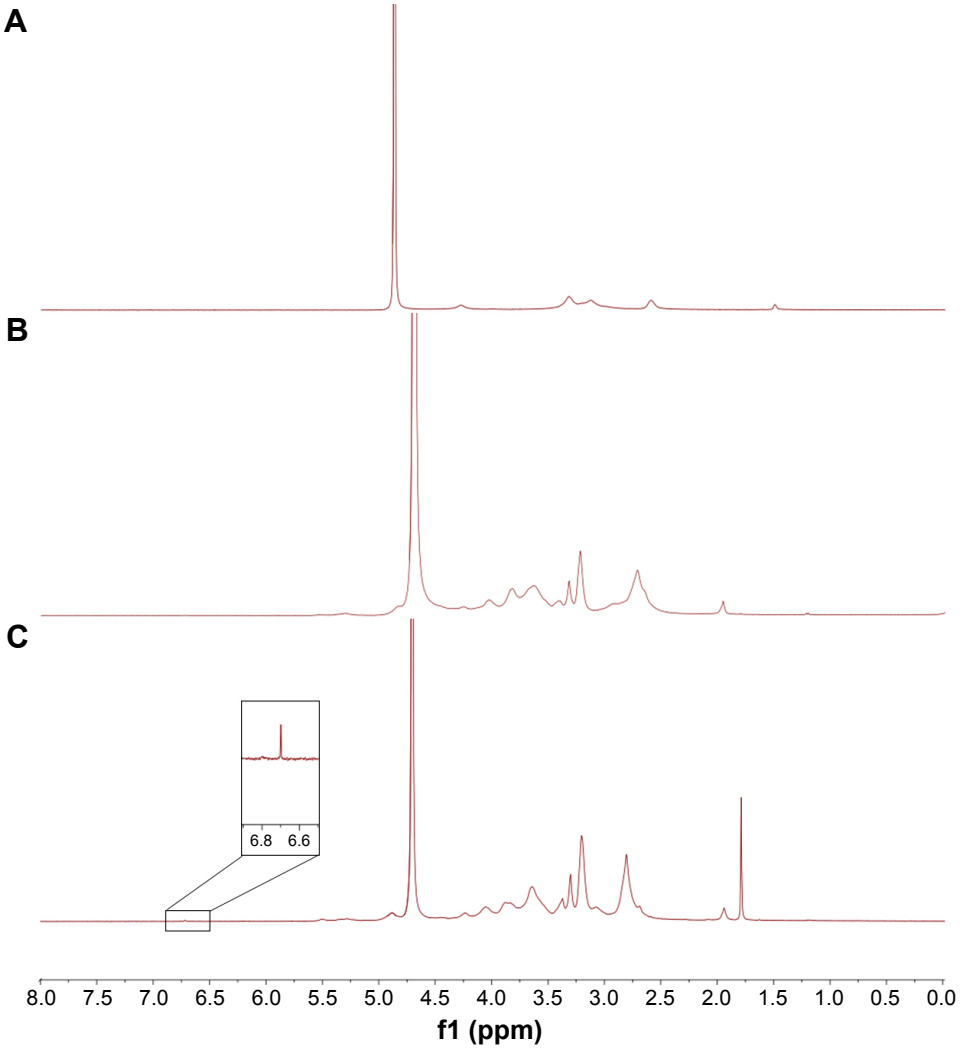

Figure 2 ^{1}H-NMR spectra of (**A**) chitosan, (**B**) TMC, and (**C**) Mal-TMC.
Abbreviations: NMR, nuclear magnetic resonance; TMC, N-trimethylated chitosan; Mal-TMC, maleimide–TMC.

chitosan were 4.26 (1H), 3.0–3.5 (2H–6H), and 2.59 (NH_2). Figure 2B shows that the chemical shifts of TMC were 5.2–5.7 (1H), 3.4–3.9 (3H–6H), 4.05 (2H), 2.71 [$-N(CH_3)_2$], and 3.23 [$-N(CH_3)_3$], indicating successful synthesis of TMC.[34] In Figure 2C, the peak at δ 6.70 is the characteristic peak of Mal, demonstrating successful introduction of the maleimide group.[35] The degree of quaternization of TMC was 27.9%, which was similar to a previous study.[34] Content analysis by HPLC showed that the incorporation efficiency of Mal with TMC was 11.3%±2.5%.

Preparation and characterization of NPs

Box–Behnken design

According to the principles of response surface methodology (RSM), using the Box–Behnken design, 17 tests were designed, and the corresponding dependent variables are shown in Table 2. Design-Expert 8.0.6 software was used to perform regression analysis using various indices and to delineate the interactions between the three independent factors. Polynomial equations between independent and dependent variables were constructed using Design-Expert 8.0.6 software.

$$Y_1 = +78.69 + 10.00A - 6.94B - 7.27C - 4.74AB + 11.95BC - 32.23A^2 - 20.99B^2 - 24.52C^2 \quad (5)$$

The regression equation for the EE had a *p*-value of less than 0.001, indicating clear significance. Moreover, lack-of-fit analysis (p=0.1523) revealed that the equation was a good fit and predictive of the relationship between the factors and EE. Among the factors, A, B, C, AB, BC, A^2, B^2, and C^2 had a significant effect on the EE.

$$Y_2 = 122.60 + 21.86A + 6.39B - 16.03C + 10.37AB - 6.80AC - 6.80BC + 28.74A^2 + 8.54B^2 + 23.81C^2 \quad (6)$$

Table 2 Effect of independent variables on dependent variables

Run	Independent variables			Dependent variables	
	Polymer concentration (mg/mL) (*A*)	Theoretical drug loading (%) (*B*)	PVA concentration (mg/100 mL) (*C*)	Entrapment efficiency (%) (Y_1)	Diameter of particles (nm) (Y_2)
1	2.5	15	1.5	4.25	140
2	10	15	1.5	28.57	175
3	6.25	15	1	77.90	124
4	2.5	15	0.5	18.58	161.7
5	6.25	5	1.5	19.00	138.5
6	10	5	1	46.78	165
7	6.25	5	0.5	60.92	153.7
8	6.25	15	1	79.31	123
9	10	15	0.5	36.34	223.9
10	10	25	1	23.12	193.6
11	6.25	25	0.5	23.45	185
12	2.5	5	1	18.34	146.9
13	6.25	15	1	76.02	119
14	6.25	15	1	80.01	121
15	6.25	25	1.5	29.34	142.6
16	6.25	15	1	80.22	126
17	2.5	25	1	13.63	134

Abbreviation: PVA, polyvinyl alcohol.

The regression equation for the particle diameter was very significant ($p<0.001$), whereas the lack of fit was not significant ($p=0.0695$). Factors A, B, C, AB, AC, BC, A^2, B^2, and C^2 had a significant effect on particle diameter.

Based on realistic clinical practice and test requirements, the optimal EE tends to be the maximum and the particle diameter tends to be minimum.[5] The regression model was further processed to determine the level of interaction between the three factors. The effect of the interaction between the various factors on the desired encapsulation efficiency and particle diameter is shown in Figure 3. The oval and steep slopes in the response surface correspond to a significant interaction between the two factors. As indicated by the sign of the highest point of the response surface, the highest response value was within the selected range of each factor. According to the expected constraint in the range of independent variables, the minimum and maximum constraint conditions of particle diameter and EE were selected, respectively.[20] The optimal formulation (A =6.13 mg/mL, B =12.98%, C =1.00 mg/100 mL, predicted response to Y_1 =78.78%, and Y_2 =120.94 nm) was selected by the desired factors. The response of the optimized recipe Y_1 (77.0%±3.9%) and Y_2 (125.4±9.1 nm) values was consistent with the predicted values generated by RSM, and the results confirmed the effectiveness of the RSM model.

Characterization of NPs

The average diameter, polydispersity index, and zeta potential of the NPs are shown in Table 3. The average diameters of TMC and Lf-TMC NPs were increased compared with that of PLGA NPs because of the modification with TMC and the coupling of Lf. However, their average diameters were still less than 200 nm, which is an important factor for transcellular transport to olfactory neurons and then to the brain.[5] The polydispersity index of all NPs indicated a narrow particle size distribution. PLGA NPs had a negative zeta potential, whereas TMC-modified NPs were positively charged, indicating that the PLGA NPs were successfully modified with TMC.[12] The encapsulation efficiency of all NPs was more than 70%. The conjugation efficiency of Lf was 16.2%±3.0%.

In vitro drug release study

The in vitro release of HupA from NPs was evaluated in 0.1 M PBS (pH 7.4). As depicted in Figure 4, free HupA was rapidly released from the dialysis bag within 4 h. In comparison, 89.3%±4.2%, 71.9%±6.0%, and 74.5%±4.5% of HupA were released from PLGA, TMC, and Lf-TMC NPs at 48 h, respectively, indicating that the NPs achieved sustained release of HupA.

Adsorption of mucin onto NPs

Adsorption of mucin onto NPs was determined by calculating the binding efficiency of mucin to NPs, as shown in Figure 5. The binding efficiencies of mucin to TMC NPs (83.2%±3.8%) and Lf-TMC NPs (86.9%±1.8%) were significantly higher than that of PLGA NPs (32.1%±2.5%) ($p<0.01$), indicating excellent adhesion of the TMC-modified

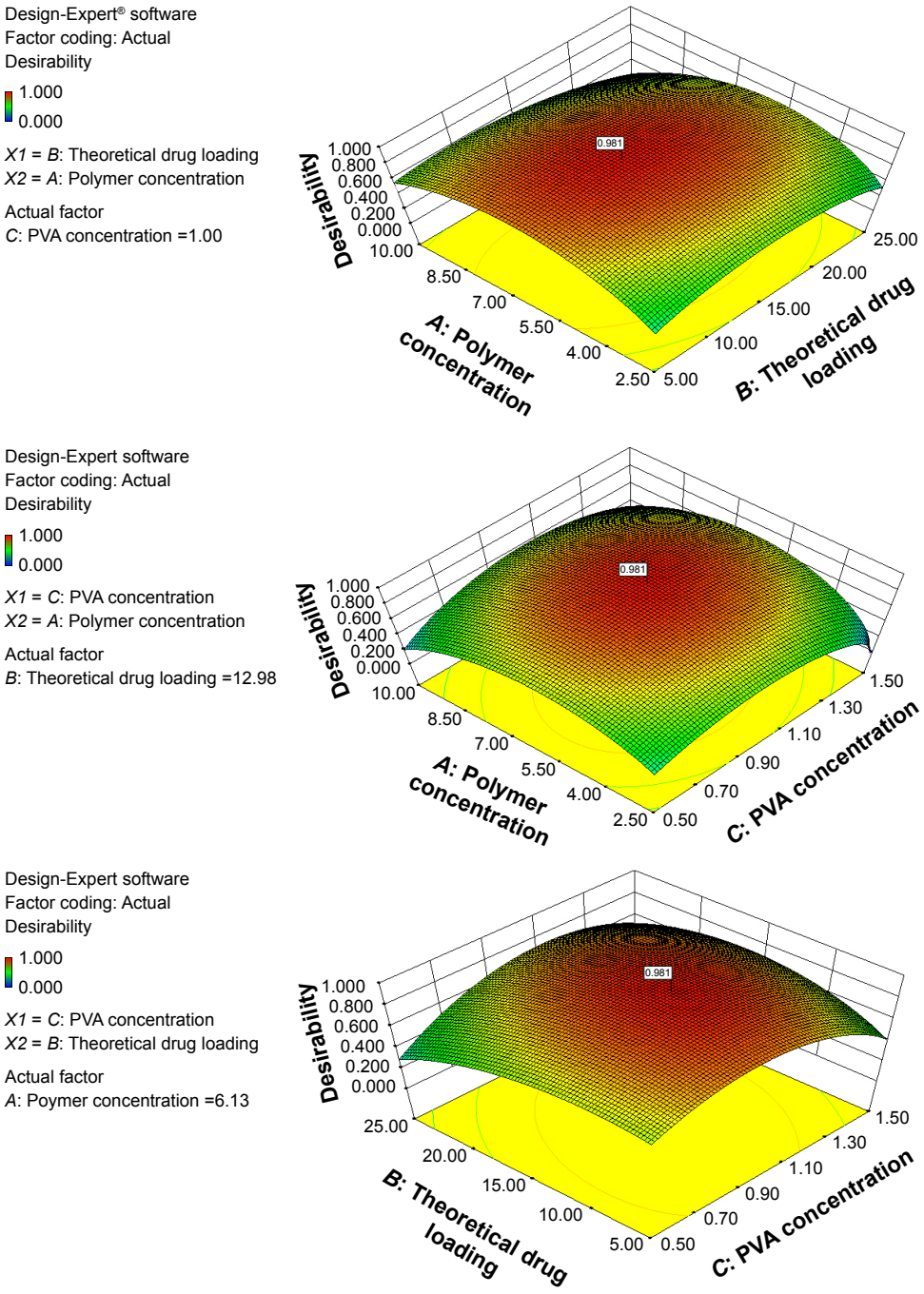

Figure 3 3D response surface plots showing the effect of independent variables on dependent variables. The y-axis represents the desirability of dependent variables. The sign represents the site of the optimal formulation.
Abbreviation: PVA, polyvinyl alcohol.

Table 3 Characterization of Huperzine A-loaded nanoparticles

Formulation	Diameter of particles (nm)	Polydispersity index	Zeta potential (mV)	Entrapment efficiency (%)
PLGA NPs	78.1±3.7	0.182±0.027	−21.2±0.8	83.2±9.2
TMC NPs	125.4±9.1	0.197±0.025	+36.3±4.0	77.0±3.9
Lf-TMC NPs	153.2±13.7	0.229±0.078	+35.6±5.2	73.8±5.7

Note: Values represent the mean ± SD (n=3).
Abbreviations: PLGA, polylactide-co-glycoside; NPs, nanoparticles; TMC, N-trimethylated chitosan; Lf, lactoferrin.

NPs.[11,39] Moreover, Lf modification did not alter its mucoadhesive characteristics.

Cytotoxicity of NPs

Following intranasal administration, NPs come into contact with nasal epithelial cells, which is the first barrier that NPs must overcome to reach the brain.[40] To emulate these conditions and evaluate the safety and uptake of NPs, the

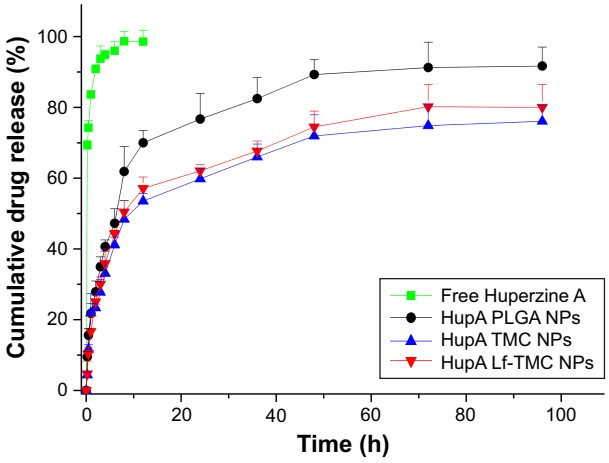

Figure 4 In vitro release study of HupA from free Huperzine A, HupA PLGA NPs, HupA TMC NPs and HupA Lf-TMC NPs in 0.1 M pH 7.4 PBS.
Abbreviations: HupA, Huperzine A; PLGA, polylactide-co-glycoside; Lf, lactoferrin; TMC, N-trimethylated chitosan; NPs, nanoparticles; PBS, phosphate buffered saline.

human bronchial epithelial cell line 16HBE was used as a model of nasal mucosa cells.[18,20] Figure 6A shows that PLGA, TMC, and Lf-TMC NPs were nontoxic to 16HBE cells at low nanocarrier concentrations. However, exposure to a higher concentration (20 mg/mL) of TMC and Lf-TMC NPs for 24 h resulted in a significant decrease ($p<0.05$) in cell viability compared with the control group, indicating that TMC-modified NPs exhibited cytotoxicity at a high concentration. This effect may be due to the high positive surface potential of TMC-modified NPs.[41] The results showed that the nanocarrier at concentrations of less than 10 mg/mL was not cytotoxic and would not interfere with cytotoxicity assessments of drugs. Figure 6B shows that free HupA and HupA-loaded NPs did not cause significant cell death at low concentrations (12.5–25 μg/mL). However, exposure

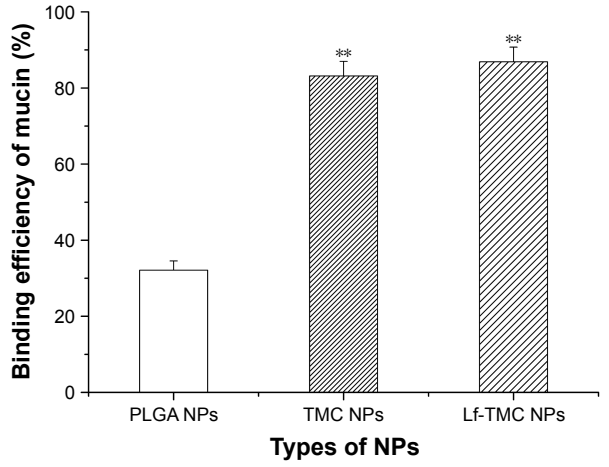

Figure 5 Binding efficiency of mucin to NPs. Values represent the mean ± SD (n=3). Statistically significant differences with PLGA NPs are marked with (**) for $p<0.01$.
Abbreviations: PLGA, polylactide-co-glycoside; Lf, lactoferrin; TMC, N-trimethylated chitosan; NPs, nanoparticles.

to higher concentrations of free HupA (50–200 μg/mL) for 24 h resulted in a significant decrease in cell viability compared with the same concentration of HupA NPs. This result indicates that the cytotoxicity of HupA was significantly reduced by encapsulation in NPs, which may be attributed to the slow release of HupA from NPs.[20] No significant difference was observed between PLGA NPs and TMC or Lf-TMC NPs, indicating that Lf and TMC were nontoxic at the experimental concentrations.

Cellular uptake of NPs

Cellular uptake of NPs by 16HBE and SH-SY5Y cells was qualitatively measured using fluorescence microscopy (Figure 7A and B) and quantitatively analyzed by flow cytometry (Figure 7C and D). SH-SY5Y cells from the human neuroblastoma cell line SK-N-S were used as a model of brain cells.[20] In Figure 7A and B, the red fluorescence is Nile red-loaded NPs and the blue fluorescence is Hoechst 33342-stained nuclei. Nile red-loaded NPs were observed around the nucleus, indicating that the NPs were taken up into the cytoplasm of 16HBE and SH-SY5Y cells. The fluorescence intensity of TMC NPs was higher than that of PLGA NPs in the cells. The same result was obtained in quantitative analysis (Figure 7C and D). The mean fluorescence of TMC NPs was very significantly higher than that of PLGA NPs ($p<0.01$). Previous studies have reported that cationic NPs are easily attracted to endothelial cells because of electrostatic interactions between the negatively charged cell membranes and positively charged cationic NPs.[10,42] In addition, the fluorescence intensity and mean fluorescence of Lf-TMC NPs were markedly higher than those of TMC and PLGA NPs, demonstrating that the Lf surface modification increased cellular uptake of NPs. These results showed that Lf-TMC NPs had a significant capacity to specifically recognize 16HBE and SH-SY5Y cells because of their greater affinity for LfR-expressing cells compared with TMC and PLGA NPs, thus promoting their uptake.[18,20]

In vivo imaging

Figure 8A shows in vivo fluorescence images of mice after intranasal administration of DiR-loaded PLGA, TMC, and Lf-TMC NPs. The fluorescence signal of TMC NPs in the brain was high and sustained over a longer period than that of PLGA NPs, suggesting that TMC modification increased nose-to-brain drug delivery and prolonged the retention time because of the mucoadhesion of TMC.[38] This property provides an extended contact time between the polymer system and the mucus surface layer to enhance drug absorption.[11,38,43] Lf-TMC NPs exhibited the highest signal in the brain

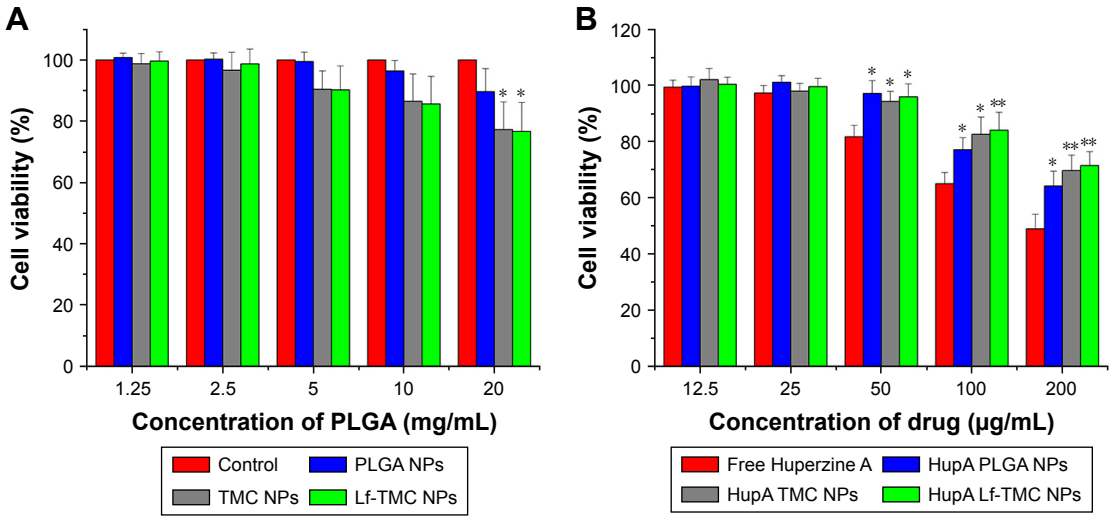

Figure 6 Cytotoxicity of free HupA, HupA loaded (**A**) and unloaded NPs (**B**) incubated for 24 h in 16HBE cells. Values represent the mean ± SD (n=3). Statistically significant differences with PLGA NPs are marked with * for $p<0.05$ and ** for $p<0.01$.
Abbreviations: HupA, Huperzine A; PLGA, polylactide-co-glycoside; Lf, lactoferrin; TMC, N-trimethylated chitosan; NPs, nanoparticles.

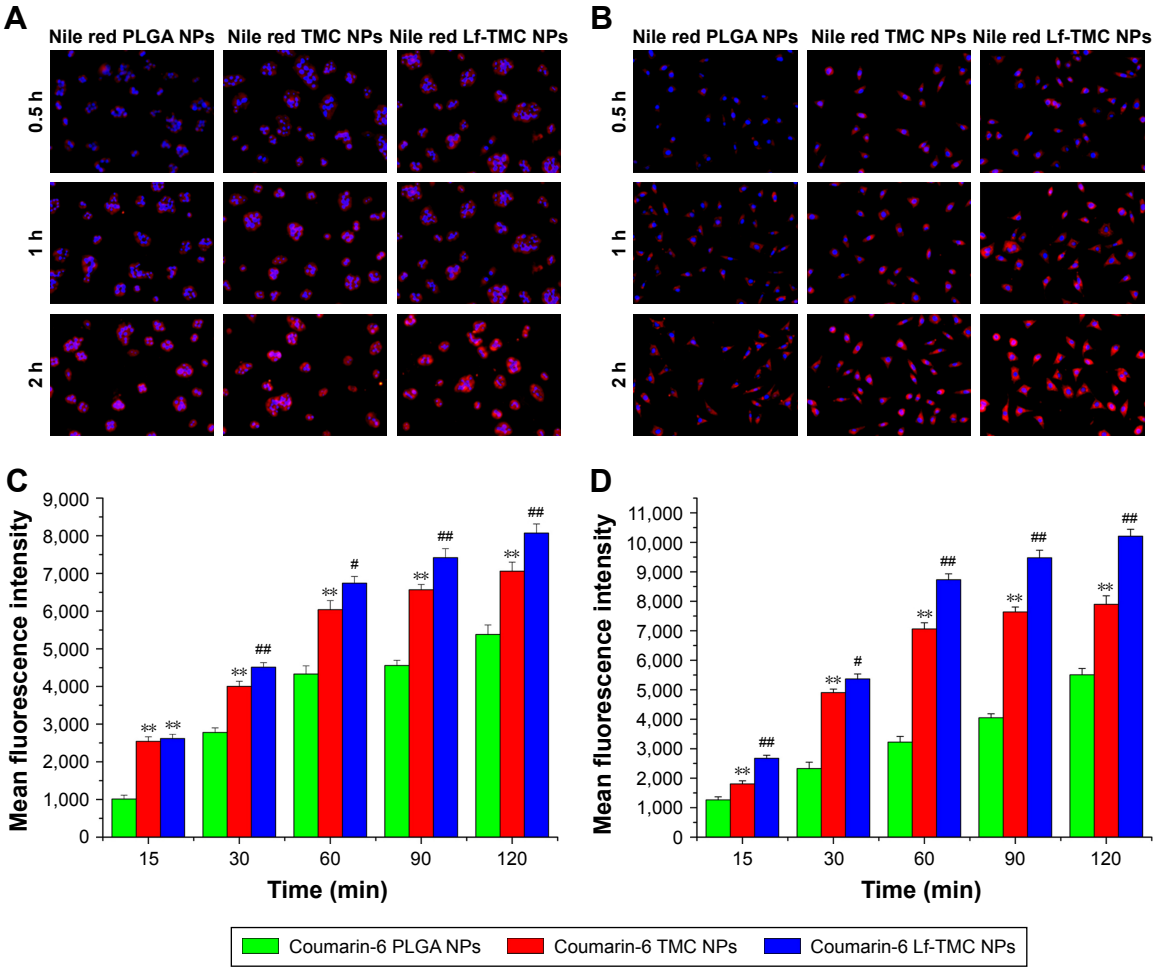

Figure 7 Cellular uptake of NPs. Fluorescence microscopy images of cellular uptake of Nile red NPs in 16HBE (**A**) and SH-SY5Y cells (**B**); original magnification ×200. Mean fluorescence intensity on flow cytometry of coumarin-6 NPs in (**C**) 16HBE and (**D**) SH-SY5Y cells. Values represent the mean ± SD (n=3). Statistically significant differences with PLGA NPs are marked with ** for $p<0.01$. Statistically significant differences with TMC NPs are marked with # for $p<0.05$ and ## for $p<0.01$.
Abbreviations: PLGA, polylactide-co-glycoside; Lf, lactoferrin; TMC, N-trimethylated chitosan; NPs, nanoparticles.

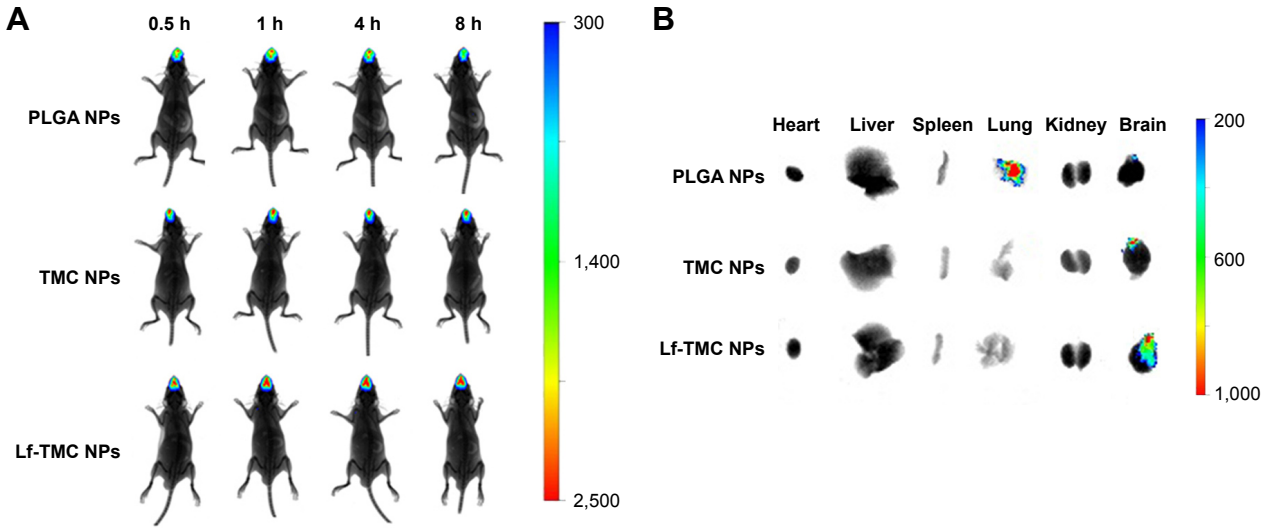

Figure 8 In vivo and ex vivo fluorescence images of organs of mice. (**A**) In vivo imaging of mice at 0.5, 1, 4, and 8 h after intranasal administration of DiR-loaded PLGA NPs, TMC NPs, and Lf-TMC NPs at a dose of 0.5 mg DiR/kg of body weight. (**B**) Ex vivo imaging of organs excised from mice at 8 h after intranasal administration.
Abbreviations: DiR, 1,1-dioctadecyl-3,3,3,3-tetramethylindotricarbocyanineiodid; PLGA, polylactide-co-glycoside; Lf, lactoferrin; TMC, N-trimethylated chitosan; NPs, nanoparticles.

compared with the other NPs. It has been reported that LfR is highly expressed on the apical surface of respiratory epithelial cells, as well as in brain endothelial cells and neurons.[15,16,44] Therefore, Lf modification increases uptake through receptor-mediated transport.[18,20]

Images of excised tissues obtained at 8 h post-administration are shown in Figure 8B. Fluorescence signals were detected in the brain of the three groups of mice, and the Lf-TMC NP group showed the highest signal. It should be noted that significant fluorescence was detected in the lungs of the PLGA NP group, which was not observed in the TMC-modified NP group. This observation may be due to the mucosal adhesion of TMC.[8] In contrast, PLGA NPs are not as readily adsorbed by nasal mucosa, leading to breathing or nasal mucociliary clearance into the lungs.[45] No fluorescence was detected in the heart, liver, spleen, or kidneys. Although in vivo imaging of NPs in mice is only qualitative, this result further highlighted that intranasal administration of TMC- and Lf-co-modified NPs increased drug-targeted delivery from the nose to brain.

Biodistribution study

The concentration–time profiles of HupA in the brain and plasma within 12 h post-intranasal administration of HupA-loaded PLGA, TMC, and Lf-TMC NPs are shown in Figure 9. The pharmacokinetic parameters following intranasal administration of HupA-loaded NPs are shown in Table 4. Upon intranasal administration of HupA-loaded NPs, the plasma concentration–time curves of HupA-loaded PLGA, TMC, and Lf-TMC NPs were similar. However, the AUC_{plasma} of Lf-TMC NPs (809.7±81.0 ng h/mL) was significantly higher than that of PLGA NPs (593.4±63.0 ng h/mL) ($p<0.05$). This result indicated that Lf-TMC NPs had greater bioavailability.[18] As depicted in Figure 9, at all time-points, the concentration of HupA in the brain of the Lf-TMC NP group was higher than that in TMC and PLGA NP groups. These results demonstrated that Lf-TMC NPs facilitated access of HupA to the brain. As shown in Table 4, the AUC_{brain} of TMC NPs was significantly higher than that of PLGA NPs. These results demonstrate that TMC modification increased the absorption of HupA entrapped in NPs in the brain, which may result from the mucoadhesive ability of TMC causing a higher concentration gradient in the nasal cavity and subsequently increased absorption of the drug.[11,43] The AUC_{brain} of Lf-TMC NPs was significantly higher than that of PLGA and TMC NPs, suggesting that intranasal administration Lf-TMC NPs resulted in stronger brain uptake owing to the presence of Lf. Lf is capable of dual targeting in the nose and brain, thus increasing nose-to-brain transport.[15,18,44] Lf-TMC NPs exhibited the highest DTI in the mouse olfactory bulb (2.0±0.1), cerebrum (with hippocampus removal) (1.6±0.1), cerebellum (1.9±0.1), and hippocampus (1.9±0.1). Furthermore, the DTIs in the olfactory bulb and hippocampus of the Lf-TMC NP group (2.0±0.1 and 1.9±0.1, respectively) showed very significant differences from those of the TMC NP group (1.6±0.1 and 1.6±0.1, respectively)

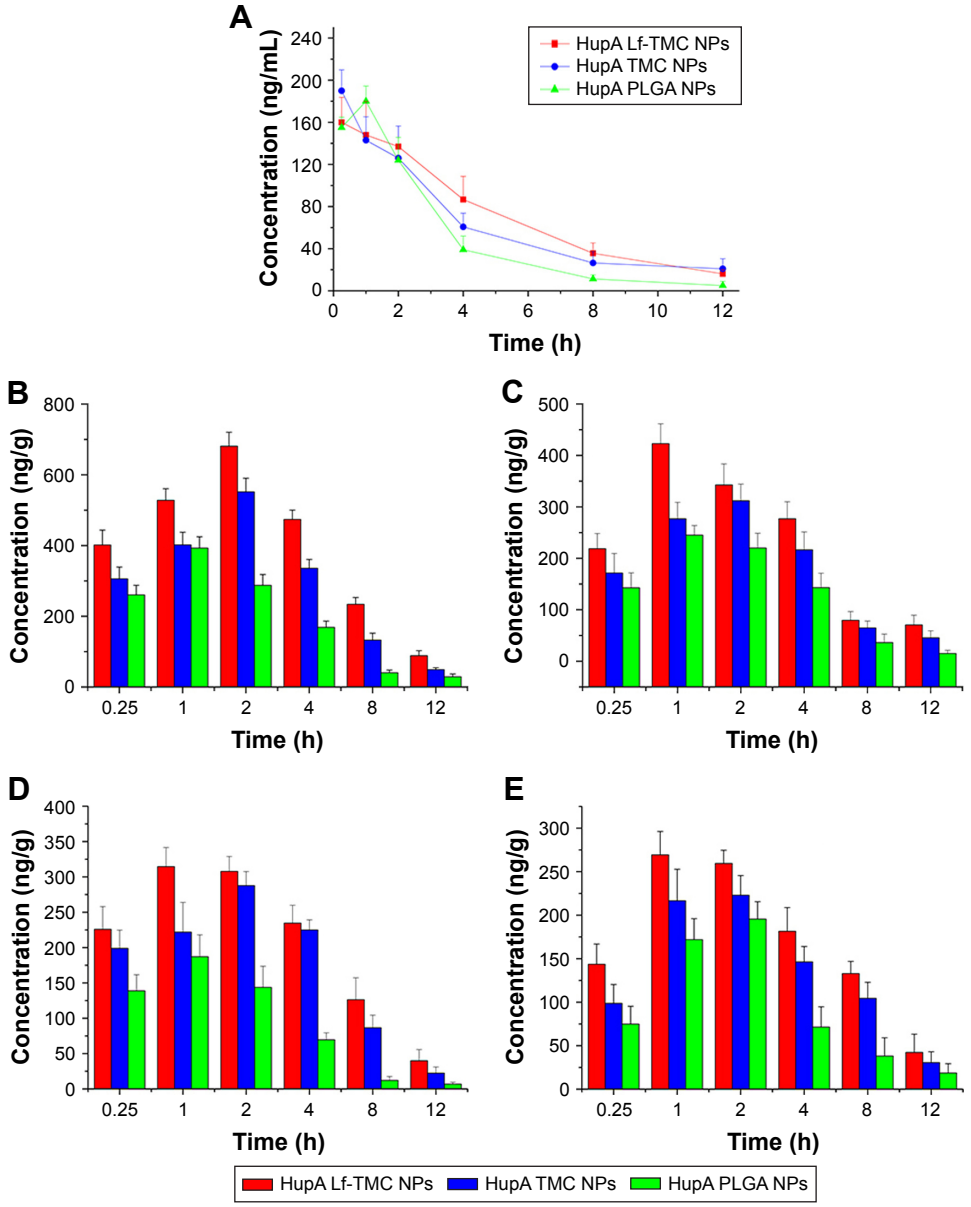

Figure 9 Brain distribution of Hup ANPs. (**A**) Blood concentration–time profiles of HupA following intranasal administration of HupA PLGA NPs, TMC NPs, and Lf-TMC NPs. Data represented the mean ± SD (n=3). Brain biodistribution of HupA following intranasal administration of HupA loaded NPs in the (**B**) olfactory bulb, (**C**) cerebrum with hippocampus removed, (**D**) cerebellum, and (**E**) hippocampus.

Abbreviations: HupA, Huperzine-A; PLGA, polylactide-co-glycoside; Lf, lactoferrin; TMC, N-trimethylated chitosan; NPs, nanoparticles.

($p<0.01$). These results indicated that the Lf modification of NPs markedly increased drug delivery to the brain, especially in the memory-related hippocampus.[18,46] The elimination rate constant (Kel) of HupA TMC NPs in plasma and the brain was smaller than that of PLGA NPs. It is likely that the attachment of TMC-modified NPs in the mouse nasal cavity resulted in sustained absorption.[39,45] The Kel of HupA Lf-TMC NPs in plasma and the brain was minimal, reflecting good pharmacokinetic properties. Such evidence strongly suggests that Lf-TMC NPs may be a promising nanocarrier for delivery of HupA from the nose to brain for AD treatment.

Conclusion

In this study, we successfully developed mucoadhesive targeted bifunctional HupA Lf-TMC NPs using the emulsion–solvent evaporation method and optimized using the Box–Behnken design. The optimized HupA Lf-TMC NPs had a suitable particle size and polydispersity index as well as a positive potential and high EE. In vitro mucin adsorption of the NPs demonstrated that Lf-TMC NPs showed high mucoadhesion. Ex vivo drug release and cell viability assays using the 16HBE cell line supported the controlled drug release and safety of the developed NPs for intranasal administration. Cellular uptake experiments showed that

Table 4 Pharmacokinetic parameters following intranasal administration of Huperzine A-loaded nanoparticles

Formulation	Tissue	Kel (h^{-1})	T_{max} (h)	C_{max} (ng/mL or ng/g)	AUC_{0-12h} (ng h/mL or ng h/g)	DTI
PLGA NPs	Plasma	0.2414	1	180.0±14.4	593.4±63.0	
	OB	0.2883	1	393.0±31.9	1,632.2±151.7	1
	CR	0.3156	1	245.1±18.6	1,120.5±133.5	1
	CL	0.2096	1	187.2±30.8	719.8±82.6	1
	HI	0.2402	2	195.6±19.9	885.0±96.4	1
TMC NPs	Plasma	0.2114	0.25	189.9±19.8	739.2±72.8	
	OB	0.1709	1	552.0±38.2	2,970.8±206.3***	1.6±0.1***
	CR	0.1957	2	312.0±32.3	1,796.2±182.9**	1.4±0.1***
	CL	0.1681	2	287.7±19.9	1,791.9±211.1**	1.8±0.1***
	HI	0.1752	2	223.1±22.5	1,491.4±130.2**	1.6±0.1***
Lf-TMC NPs	Plasma	0.1948	0.25	160.0±23.7	809.7±81.0*	
	OB	0.1884	2	681.0±39.3	4,219.6±316.7***,##	2.0±0.1***,##
	CR	0.2005	1	423.0±38.4	2,283.8±113.6***,#	1.6±0.1***
	CL	0.1902	1	314.6±27.0	2,138.9±207.4***,#	1.9±0.1***
	HI	0.1669	1	269.4±26.9	1,857.5±155.8***,##	1.9±0.1***,##

Notes: Values represent the mean ± SD (n=3). Statistically significant differences from PLGA NPs: *$p<0.05$, **$p<0.01$, ***$p<0.001$. Statistically significant differences from TMC NPs: #$p<0.05$, ##$p<0.01$.

Abbreviations: PLGA, polylactide-co-glycoside; NPs, nanoparticles; TMC, N-trimethylated chitosan; Kel, elimination rate constant; T_{max}, peak-reaching time; C_{max}, the maximum concentration; AUC, area under concentration-time curve; DTI, drug targeting index; Lf, lactoferrin; OB, olfactory bulb; CR, cerebrum with hippocampus removal; CL, cerebellum; HI, hippocampus.

Lf-TMC NPs exhibited enhanced cellular uptake compared with PLGA NPs. Lf-TMC NPs were highly distributed in the brain and over a prolonged period through the active targeting of Lf and the mucoadhesion of TMC. These results demonstrated that Lf-TMC NPs may be used as a potential drug delivery system for nose-to-brain delivery. In future studies, we will continue to evaluate their therapeutic efficacy in animal AD models.

Acknowledgments

We are thankful for financial support from the Science and Technology Project of Higher Education of Shandong Province (J16LM52) and the Natural Science Foundation of Shandong Province (ZR2017LH076).

Disclosure

Aipang Wang is affiliated with Shandong Luye Pharmaceutical Co., Ltd. The authors report no conflicts of interest in this work.

References

1. Winblad B, Amouyel P, Andrieu S, et al. Defeating Alzheimer's disease and other dementias: a priority for European science and society. *Lancet Neurol*. 2016;15(5):455–532.
2. Graham WV, Bonito-Oliva A, Sakmar TP. Update on Alzheimer's Disease Therapy and Prevention Strategies. *Annu Rev Med*. 2017;68:413–430.
3. Hampel H, Prvulovic D, Teipel S, et al. The future of Alzheimer's disease: the next 10 years. *Prog Neurobiol*. 2011;95(4):718–728.
4. Lochhead JJ, Thorne RG. Intranasal delivery of biologics to the central nervous system. *Adv Drug Deliv Rev*. 2012;64(7):614–628.
5. Mistry A, Stolnik S, Illum L. Nanoparticles for direct nose-to-brain delivery of drugs. *Int J Pharm*. 2009;379(1):146–157.
6. Kulkarni AD, Vanjari YH, Sancheti KH, Belgamwar VS, Surana SJ, Pardeshi CV. Nanotechnology-mediated nose to brain drug delivery for Parkinson's disease: a mini review. *J Drug Target*. 2015;23(9):775–788.
7. Djupesland PG. Nasal drug delivery devices: characteristics and performance in a clinical perspective-a review. *Drug Deliv Transl Res*. 2013;3(1):42–62.
8. Jafarieh O, Md S, Ali M, et al. Design, characterization, and evaluation of intranasal delivery of ropinirole-loaded mucoadhesive nanoparticles for brain targeting. *Drug Dev Ind Pharm*. 2015;41(10):1674–1681.
9. Casettari L, Illum L. Chitosan in nasal delivery systems for therapeutic drugs. *J Control Release*. 2014;190:189–200.
10. Gartziandia O, Herran E, Pedraz JL, Carro E, Igartua M, Hernandez RM. Chitosan coated nanostructured lipid carriers for brain delivery of proteins by intranasal administration. *Colloids Surf B Biointerfaces*. 2015;134:304–313.
11. Pawar D, Goyal AK, Mangal S, et al. Evaluation of mucoadhesive PLGA microparticles for nasal immunization. *AAPS J*. 2010;12(2):130–137.
12. Sheng J, Han L, Qin J, et al. N-trimethyl chitosan chloride-coated PLGA nanoparticles overcoming multiple barriers to oral insulin absorption. *ACS Appl Mater Interfaces*. 2015;7(28):15430–15441.
13. Hagenaars N, Mania M, de Jong P, et al. Role of trimethylated chitosan (TMC) in nasal residence time, local distribution and toxicity of an intranasal influenza vaccine. *J Control Release*. 2010;144(1):17–24.
14. Du PL, Kotzé AF, Junginger HE. Nasal and rectal delivery of insulin with chitosan and N-trimethyl chitosan chloride. *Drug Deliv*. 2010;17(6):399–407.
15. Suzuki YA, Lopez V, Lönnerdal B. Mammalian lactoferrin receptors: structure and function. *Cell Mol Life Sci*. 2005;62(22):2560–2575.
16. Elfinger M, Maucksch C, Rudolph C. Characterization of lactoferrin as a targeting ligand for nonviral gene delivery to airway epithelial cells. *Biomaterials*. 2007;28(23):3448–3455.
17. Qian ZM, Wang Q. Expression of iron transport proteins and excessive iron accumulation in the brain in neurodegenerative disorders. *Brain Res Brain Res Rev*. 1998;27(3):257–267.

18. Liu Z, Jiang M, Kang T, et al. Lactoferrin-modified PEG-co-PCL nanoparticles for enhanced brain delivery of NAP peptide following intranasal administration. *Biomaterials*. 2013;34(15):3870–3881.
19. Guo C, Yang ZH, Zhang S, et al. Intranasal lactoferrin enhances α-secretase-dependent amyloid precursor protein processing via the ERK1/2-CREB and HIF-1α pathways in an Alzheimer's disease mouse model. *Neuropsychopharmacology*. 2017;42(13):2504–2515.
20. Bi C, Wang A, Chu Y, et al. Intranasal delivery of rotigotine to the brain with lactoferrin-modified PEG-PLGA nanoparticles for Parkinson's disease treatment. *Int J Nanomed*. 2016;11:6547–6559.
21. Ferreira A, Rodrigues M, Fortuna A, Falcão A, Alves G. Huperzine A from *Huperzia serrata*: a review of its sources, chemistry, pharmacology and toxicology. *Phytochem Rev*. 2016;15(1):51–85.
22. Zhang HY. New insights into Huperzine A for the treatment of Alzheimer's disease. *Acta Pharmacol Sin*. 2012;33(9):1170–1175.
23. Yang G, Wang Y, Tian J, Liu JP. Huperzine A for Alzheimer's disease: a systematic review and meta-analysis of randomized clinical trials. *PLoS One*. 2013;8(9):e74916.
24. Wang ZY, Liu JG, Li H, Yang HM. Pharmacological Effects of Active Components of Chinese Herbal Medicine in the Treatment of Alzheimer's Disease: A Review. *Am J Chin Med*. 2016;44(08):1525–1541.
25. Ma T, Gong K, Yan Y, et al. Huperzine A promotes hippocampal neurogenesis in vitro and in vivo. *Brain Res*. 2013;1506:35–43.
26. Huang XT, Qian ZM, He X, et al. Reducing iron in the brain: a novel pharmacologic mechanism of Huperzine A in the treatment of Alzheimer's disease. *Neurobiol Aging*. 2014;35(5):1045–1054.
27. Wang CY, Zheng W, Wang T, et al. Huperzine A activates Wnt/β-catenin signaling and enhances the nonamyloidogenic pathway in an Alzheimer transgenic mouse model. *Neuropsychopharmacology*. 2011;36(5):1073–1089.
28. Yue P, Tao T, Zhao Y, Ren J, Chai X. Huperzine A in rat plasma and CSF following intranasal administration. *Int J Pharm*. 2007;337(1–2):127–132.
29. Tao T, Zhao Y, Yue P, Dong WX, Chen QH. [Preparation of Huperzine A nasal in situ gel and evaluation of its brain targeting following intranasal administration]. *Acta Pharm Sin*. 2006;41(11):1104–1110. Chinese.
30. Zhang L, Han L, Qin J, Lu W, Wang J. The use of borneol as an enhancer for targeting aprotinin-conjugated PEG-PLGA nanoparticles to the brain. *Pharm Res*. 2013;30(10):2560–2572.
31. Li F, Hu R, Wang B, et al. Self-microemulsifying drug delivery system for improving the bioavailability of Huperzine A by lymphatic uptake. *Acta Pharm Sin B*. 2017;7(3):353–360.
32. Patel PA, Patil SC, Kalaria DR, Kalia YN, Patravale VB. Comparative in vitro and in vivo evaluation of lipid based nanocarriers of Huperzine A. *Int J Pharm*. 2013;446(1–2):16–23.
33. Zhao Y, Yue P, Tao T, Chen QH. Drug brain distribution following intranasal administration of Huperzine A in situ gel in rats. *Acta Pharmacol Sin*. 2007;28(2):273–278.
34. Hu XJ, Liu Y, Zhou XF, et al. Synthesis and characterization of low-toxicity N-caprinoyl-N-trimethyl chitosan as self-assembled micelles carriers for osthole. *Int J Nanomed*. 2013;8:3543–3558.
35. Liu Q, Zheng X, Zhang C, et al. Antigen-conjugated N-trimethylaminoethylmethacrylate chitosan nanoparticles induce strong immune responses after nasal administration. *Pharm Res*. 2015;32(1):22–36.
36. Sharma D, Sharma RK, Sharma N, et al. Nose-To-Brain Delivery of PLGA-Diazepam Nanoparticles. *AAPS PharmSciTech*. 2015;16(5):1108–1121.
37. Huwyler J, Wu D, Pardridge WM. Brain drug delivery of small molecules using immunoliposomes. *Proc Natl Acad Sci U S A*. 1996;93(24):14164–14169.
38. Yin Y, Chen D, Qiao M, Lu Z, Hu H. Preparation and evaluation of lectin-conjugated PLGA nanoparticles for oral delivery of thymopentin. *J Control Release*. 2006;116(3):337–345.
39. Kumar M, Pandey RS, Patra KC, et al. Evaluation of neuropeptide loaded trimethyl chitosan nanoparticles for nose to brain delivery. *Int J Biol Macromol*. 2013;61(10):189–195.
40. Pires A, Fortuna A, Alves G, Falcão A. Intranasal drug delivery: how, why and what for? *J Pharm Pharm Sci*. 2009;12(3):288–311.
41. Bhattacharjee S, Ershov D, van der Gucht J, et al. Surface charge-specific cytotoxicity and cellular uptake of tri-block copolymer nanoparticles. *Nanotoxicology*. 2013;7(1):71–84.
42. Drin G, Cottin S, Blanc E, Rees AR, Temsamani J. Studies on the internalization mechanism of cationic cell-penetrating peptides. *J Biol Chem*. 2003;278(33):31192–31201.
43. Critchley H, Davis SS, Farraj NF, Illum L. Nasal absorption of desmopressin in rats and sheep. Effect of a bioadhesive microsphere delivery system. *J Pharm Pharmacol*. 1994;46:651–656.
44. Suzuki YA, Lopez V, Lönnerdal B. Mammalian lactoferrin receptors: structure and function. *Cell Mol Life Sci*. 2005;62(22):2560–2575.
45. Muntimadugu E, Dhommati R, Jain A, Challa VG, Shaheen M, Khan W. Intranasal delivery of nanoparticle encapsulated tarenflurbil: a potential brain targeting strategy for Alzheimer's disease. *Eur J Pharm Sci*. 2016;92:224–234.
46. Bannerman DM, Rawlins JN, Mchugh SB, et al. Regional dissociations within the hippocampus – memory and anxiety. *Neurosci Biobehav Rev*. 2004;28(3):273–283.